# Beam tests of a double-sided silicon strip detector with fast binary readout electronics before and after proton-irradiation


Y. Unno[a], M. Takahata[h], H. Maeohmichi[h], F. Hinode[a], T. Akagi[a], T. Aso[b], M. Daigo[c], J. DeWitt[d], D. Dorfan[d], T. Dubbs[d], M. Frautschi[e], A. Grillo[d], C. Haber[f], T. Handa[g], T. Hatakenaka[h], B. Hubbard[d], H. Iwasaki[a], Y. Iwata[g], D. Kaplan[i], S. Kashigin[d], I. Kipnis[f], S. Kobayashi[j], T. Kohriki[a], T. Kondo[a], W. Kroeger[d], J. Matthews[k], H. Miyata[b], A. Murakami[j], K. Noble[d], K. O'Shaughnessy[d], T. Ohmoto[g], T. Ohsugi[g], H. Ohyama[g], T. Pulliam[d], J. Rahn[d], W.A. Rowe[d], H.F.-W. Sadrozinski[d], A. Seiden[d], J. Siegrist[f], E. Spencer[d], H. Spieler[f], R. Takashima[l], N. Tamura[h], S. Terada[a], M. Tezuka[j], A. Webster[d], R. Wichmann[d], M. Wilder[d], M. Yoshikawa[g]

[a] *Department of Physics, KEK, Tsukuba, Ibaraki 305, Japan*

[b] *Department of Physics, Niigata University, Niigata 950-21, Japan*

[c] *Department of Economics, Toyama Univeristy, Toyama 930, Japan*

[d] *SCIPP, University of California, Santa Cruz, CA 95064, USA*

[e] *Department of Physics, Texas Tech Univeristy, Lubbock, TX 79409-1051, USA*

[f] *Department of Physics, LBNL, Berkeley, CA 94720, USA*

[g] *Department of Physics, Hiroshima University, Higashi-Hiroshima 724, Japan*

[h] *Department of Physics, Okayama University, Okayama 700, Japan*

[i] *Department of Physcis, University of Oklahoma, Norman, OK 73019, USA*

[j] *Department of Physics, Saga University, Saga 840, Japan*

[k] *Department of Physics, University of New Mexico, Albuquerque, NM 87131, USA*

[l] *Department of Education, Kyoto University of Education, Kyoto 612, Japan*



A double-sided silicon strip detector with a radiation-tolerant design was fabricated and characterized in a sequence of beam tests at KEK using 4 GeV/c pions. The detectors were combined with newly designed, fast, lower power, bipolar amplifier-shaper-discriminator chips and CMOS digital pipeline chips to record hit-no hit signals in the strips. The responses were measured before and after the proton irradiation at a equivalent fluence of $1{\times}10^{14}$ p/cm$^2$ in efficiencies, noise occupancies, spatial resolutions, presented focusing on incident angle and strip-pitch dependence. The median pulse height distribution extracted from the threshold scan of the efficiency enabled to understand the response. A 1 Tesla magnetic field enabled to extract the Hall mobilities of electrons and holes.


## I. INTRODUCTION

Silicon strip detectors have been proposed to be used as a precision tracking and vertexing device in high-energy-physics experiments[1]. In an experiment in a super high energy proton-proton collisions, such as ATLAS[2] in LHC[3], one major concern is the tolerance to the high radiation environment. The ATLAS silicon strip detector anticipates a cumulative fluence of more than $10^{14}$ charged particles/cm$^2$ over the lifetime of 10 years.

A number of studies has been executed to understand the radiation effect to the silicon strip detectors[4] and a double-sided silicon strip detector (DSSD) has been produced with a radiation tolerant design[5]. The latest specification of the design is summarized in Table 1. The axial strips were processed in the n-side, and the stereo strips (10 mrad stereo-angle) in the p-side, with a strip pitch of 50 µm. The implant strips were AC-coupled to aluminum readout-electrodes, sandwiching thin $SiO_2$ and SiN insulators. A goal of the design was to operate the detector at a bias voltage up to 200V, while grounding the readout electrodes, before and after the type inversion of the silicon bulk due to the radiation damage.

A simple, fast, and low-power electronics was developed to read out the strip detectors[6]. High speed was required to tag a event to the bunch crossing and to keep occupancy low. The bunch crossing will occur at 40 MHz in the collider. Low power was required to make the cooling of a large system manageable. A system could be over several millions of channels. The readout scheme was a simple "Binary-readout" that registered only hit and no-hit information in a channel for the pulse height above a threshold. The one-bit of data were stored in a digital pipeline until a trigger arrived.

Along with developing a radiation-tolerant silicon strip detector, understanding of the detector response before and after radiation damage was an urgent task. A combination of the DSSD and the binary readout electronics was beam-tested at KEK using 4 GeV pions from its 12 GeV proton synchrotron, for proof of principle, and subsequently, for characterization of improved versions before irradiation (T280, T330). To characterize the detector after radiation damage, the DSSD was irradiated with protons at TRIUMF and at LBNL, and then, beam-tested at KEK(T355)[7].

In previous reports[8,9], we have presented the responses of the non-irradiated and irradiated detectors mainly to normal incident particles. In the ATLAS layout of the silicon tracking system, charged tracks of 1GeV/c momentum hit the detector at an angle of 10° at a radius of 60cm perpendicular to the axial strips because of the 2 Tesla magnetic field, in addition to a tilt angle of the detectors. The charges, i.e., electron and hole pairs, generated along a inclined track in the silicon bulk will split into two or more strips. This charge splitting may lead to inefficiency depending on the incident angle and a threshold of the binary electronics.

The detector-under-test (DUT) had a basic readout pitch of 50µm. A readout region was arranged to have readout pitches such as 100µ and 150µ to evaluate the response to other pitch configurations. In this report, we will describe the incident angle and pitch-configuration dependence of the responses of the DSSD with the fast binary readout electronics.

Table 1. Specification of the radiation-hard double-sided silicon strip detector. Two fabrications: DSSD1 with the standard implant-process parameters and DSSD2 with an improved ones[b].

| | |
|---|---|
| (1) Substrate | |
| Type | n-type Si |
| Resistivity | 4~8 kΩ·cm |
| Thickness | 300±10 µm |
| (2) Size | |
| Overall dimension[a] | 60 mm×34.1 mm |
| Stereo-effective area | 58.8 mm×31.4 mm |
| (3) Strip | |
| Axial strips | n-side |
| Stereo strips | p-side |
| Pitch | 50 µm |
| Stereo angle | 10 mrad |
| Implant width | 12 µm |
| Implant depth[b] | >1µm, round edge |
| AC electrode width | <10 µm |
| Strip isolation on n-side | common p-implant |
| (4) AC coupling | |
| Insulator | $SiO_2$+SiN |
| (5) Bias resistor | |
| Polycrystalline silicon | 250±50 kΩ |

[a] Actual dimension is 60 µm narrower due to sawing

## II. EXPERIMENT

### A. Setup

Three, T280, T330, and T355, were set up at the π2 test beam line of the 12-GeV proton synchrotron at KEK. Three scintillation counters, $S_1$, $S_2$, $S_3$, were set in the upstream of the detectors to make a trigger for 4 GeV negative pions to initiate a data-acquisition sequence. The $S_1$, $S_2$, and $S_3$ had a size of 2 cm (width) × 2 cm (height) × 5 mm (thickness). The $S_2$ and $S_3$ were placed nearby but displaced to make a smaller overlapping region: 2 cm×1 cm by displacing vertically or 1 cm×1 cm by displacing diagonally. The $S_1$ was set 3 to 4 m upstream and the $S_2$•$S_3$ at about 1m upstream of the detectors. Two additional small counters, $F_1$ and $F_2$, slightly wider than the readout area, were placed in front and back of the detectors, for limiting the trigger area, checking the alignment of the detectors and consistency of the counts in the counters and the detectors, etc. The $F_1$ and $F_2$ counters were read out with optical fibers to allow their placement in a magnetic field. Two Cerenkov counters were used occasionally to differentiate pions and electrons (the fraction of electrons was a few % of the total particles). The coordinate system defined was right-handed: $+z$ in the beam-flow and $+y$ in the vertically upward direction.

The silicon strip detectors were placed on a translation-rotation stage inside an aluminum box . The box, 60 cm (width)×39 cm (height)×65 cm (depth), shielded the detectors electrically and optically and made a cooled environment for the electronics with an forced flow of air. The translation-rotation stage was set in the box to move the detectors in the $x$-direction, rotate in the $\phi$ angles around the $y$-axis, the $\theta$ angles around the rotated $x$-axis. The direction of the detector strips was set in vertical. In the $\phi$ angle rotations, two types of methods were employed: in the beam test of small rotations, only the stage was rotated (Fig. 1(A)); in the beam test of larger rotations the detectors were stepped with extra fixtures in addition to the rotations since the readout region was limited (Fig. 1(B)). In T230, a magnetic field was provided up to 1.0 Tesla vertically (direction towards $-y$) by a dipole magnet (USHIWAKA) which had an opening aperture of 82 cm(W) × 40 cm(H) × 70 cm(D).

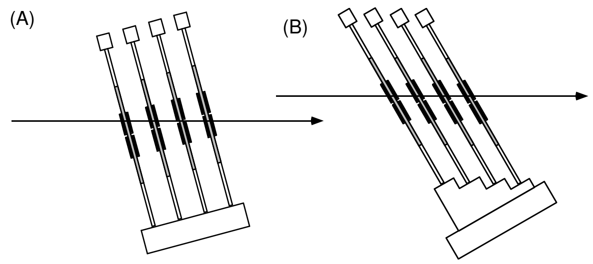


Fig. 1 Rotation schemes: (A) rotation of the stage for a small rotation angles, (B) with extra stepping fixtures for larger rotation angles. Several types of the stepping fixtures were prepared for different angles.

Three planes of detectors in T280 and four planes in T330 and T355 were set and aligned in a mini-crate on the translation-rotation stage. A schematic presentation of a setting is shown in Fig. 2. The detector planes were separated by 8mm for the multiple-scattering effect to be minimized. For 4 GeV/c pions, the r.m.s. deviation of the hit in the middle plane out of the straight line connecting the hits in the adjacent planes was calculated to be 0.3µm due to the 300µ silicon material in the middle plane.

The most-upstream and the most-downstream silicon detectors were the anchors and the inner two detectors were the detector-under-test(DUT). The anchor and the DUT detectors were the same double-sided silicon strip detectors as summarized in Table 1. The anchor detectors had an identical strip-pitch arrangement and were non-irradiated. The DUT1 (LBIC-DUT) was the one tested before and after proton irradiation and having several strip-pitch configurations. Out of the two DUT's (LBIC-DUT and ATT-DUT) in the T330 and T355, only the results for LBIC-DUT will be presented in this report.

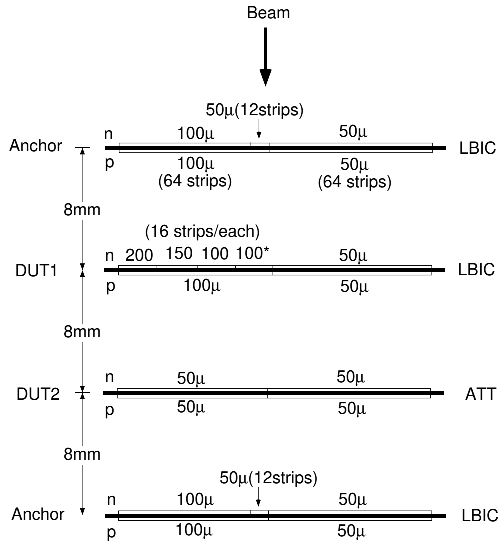


Fig. 2 Detector setup of T330 and T355. The n-side was the axial strips and the p-side the stereo strips (10 mrad. stereo angle).

The front-end electronics(FEE) consisted of a pair of two chips: a bipolar amplifier-shaper-discriminator chip, and a CMOS digital pipeline chip(CDP64) clocked at 10 or 40 MHz [10]. Three bipolar amplifier-shaper-comparator chips were used: TEKZ, LBIC and ATT, all of which had an unipolar Poisson/Gaussian shaping circuitry. TEKZ had a slow peaking time of 30ns[11]. LBIC had a fast 22ns shaping meant for the 40 MHz operation[6]. ATT had a slower peaking time but had a time-walk compensation circuitry to improve a time resolution[12]. Due to a two-level buffers in the digital pipeline chips, the analog signal processing and the digital buffering in the pipeline with a clock were functioning simultaneously. The simultaneous data acquisition, i.e. existence or non-existence of a clock pickup, was one of the issues of the beam test. All detectors were instrumented only in the central part of the double sides with two pairs of 64channel FEEs (6.4 mm width). The setups used for three are summarized in Table 2.

A schematic drawing of the detector-electronics chain is presented in Fig. 3. The detector is symbolically drawn by the diode. In the detector and binary-readout electronics, performance can be controlled by two parameters: a detector bias voltage for depleting the detector, and a threshold of the discriminator for counting hit-no hit. Although there was one threshold in the binary system, it was possible to extract analog information by scanning the threshold.

Table 2. A summary of the beam test setups

| | Number of detectors | Detector type | Front-end Electronics | Clock [MHz] | Rotation stage |
|---|---|---|---|---|---|
| T290 | 3 | DSSD1 | TEKZ | 10 | (A) |
| T330 | 4 | Non-irrad-DSSD2 | LBIC, ATT | 40 | (B) |
| T355 | 4 | Irrad-DSSD2 | LBIC, ATT | 40 | (B) |

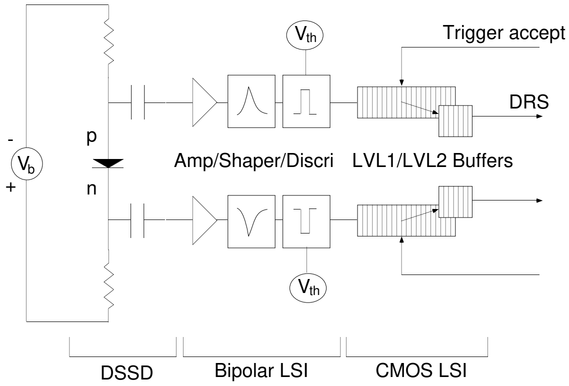


Fig. 3 Schematic representation of the DSSD and binary FEE chain. There are two parameters to control the chain: a bias voltage and a threshold of the discriminator.

## *B. Data Acquisition*

The data acquisition (DAQ) was done using a VME-UNIX DAQ system(UNIDAQ)[13]. A UNIX workstation (DEC station 5000/125) communicated with VME modules through the DEC Turbo-channel VME adapter in the workstation and the DEC PMABV-T6000-AA VME module in a VME crate. CAMAC modules were communicated via VME.

The communication between VME and the FEE on the detector was made through a VME module called the digital readout sequencer (DRS)[14]. The DRS also received clock, threshold voltage, and calibration signals and routed to the detectors. The difference (in time) of a trigger and the clock was measured with a CAMAC TDC.

## *C. Ganging Case definitions*

To characterize the detector performance as a function of strip-pitch, the detector strips were wire-bonded to the FEE channels in several configurations. In one chip set, all strips were bonded to the FEE channels with the 50μ pitch. In the other chip set on the p-side, two strips were ganged into one FEE channel, giving a 100μ pitch. On the n-side of the LBIC-DUT, a chip set was bonded into four configurations: alternate bonding with intermediate strips unbonded, thus giving a case of one intermediate floating-strip readout (100*μ), adjacent two strips being ganged into one channel(100μ), three strips into one channel(150μ), and four strips into one channel(200μ). The connection of the detector strips and the electronics channels are shown graphically in Fig. 4. The case classifications of the DUT and the anchor pitches are summarized in Table 3. Although subtleties such as the electric field lines, input capacitance of a channel, are different between the ganged-strip pitches and wide-spacing single-strip pitches, the performance of these configurations would be a good guideline of the strip pitches.

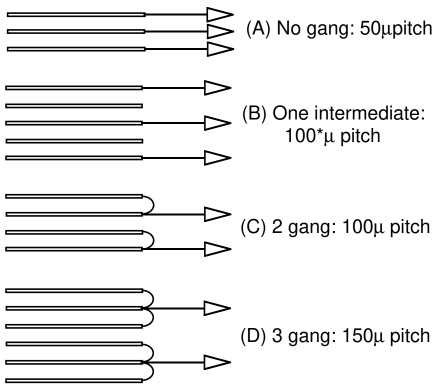


Fig. 4 Graphical representation of the ganging of detector strips into FEE channels (triangle) on the n-side of the LBIC-DUT in T330 and T355.

Table 3. Ganging-case classification

| Case | Ganging | DUT Pitch [μm] | Anchor pitch [μm] |
|---|---|---|---|
| 50μ | No | 50 | 50 |
| 100*μ | One-intermediate | 100 | 50 |
| 100μ | 2 | 100 | 100 |
| 150μ | 3 | 150 | 100 |

## *D. Proton Irradiation*

The LBIC-DUT of the T330 was irradiated to protons at TRIUMF and at LBNL. The fluence at TRIUMF was below $10^{13}$ p/cm$^2$. The LBNL irradiation was a spot of a diameter of 1.5cm at the peak. The maximum fluence in the instrumented area was estimated to be $4.6\times10^{13}$ p/cm$^2$. In order to get higher damage, the DUT was warmed up for the anti-annealing to be expedited: the expected damage level at the time of the beam test (T355) was estimated to be equivalent to a fluence of $1\times10^{14}$ p/cm$^2$ in depletion voltage (120V estimated). Since the spot was much smaller than the detector size (6cm×3.4cm), the fluence along the instrumented strips was quite non-uniform: over the 6cm strip, the peak of the fluence was at y~4.2cm where the bulk type was inverted (from the initial n-type to the p-type), the intrinsic bulk at around y~1.5cm. Details of the proton irradiation and the fluence profile can be found in the ref. 9.

## *D. Data summary*

Parameters varied in the three were: (1) bias voltage, (2) threshold, (3) incident angles in the $\phi$ and $\theta$ directions where the $\phi$ direction was the angle perpendicular to the strip directions, (4) magnetic field. In T280, the incident angles and the magnetic field were varied; in T330 and T355, the bias voltage, threshold, and $\phi$ angles. There was no magnetic field in these two tests. The range of variations are summarized in Table 4. The parameter variation was diagonalized most of the time, i.e., only one parameter was varied at a time. The T280 and T330 data were for non-irradiated and T355 for the irradiated detector.

Table 4. Summary of the data taken in T280, T330, and T355

| | Bias voltage [V] | Threshold [fC] | Incident angles $\phi$ [°] | $\theta$ [°] | Magnetic field [T] |
|---|---|---|---|---|---|
| T280 | 100 | [a]1.2/0-6 | 0-9 | 0-54 | 0,1 |
| T330 | 60-120 | 0-2 | 0-54 | 0 | 0 |
| T355 | 40-160 | 0-6 | 0-45 | 0 | 0 |

[a] Mostly at 1.2fC. x-y means the variation was from the lowest x to the highest y.

# RESULTS

## *A. Response of the irradiated detector*

In the binary electronics, a direct observable quantity is the efficiency of the signals above a threshold. In a physics experiment the threshold will be kept at a constant value for most of the experimental time. Two issues are important in a beam test: (1) to evaluate the efficiency at thresholds where a physics experiment would use, and (2) to evaluate a signal and noise behavior to access the head-room of the system. The issue (1) is direct in the beam test. The issue (2) can be evaluated, even in a binary electronics, by scanning the threshold.

The efficiency variation as a function of threshold is shown in Fig. 5(a) for the irradiated LBIC-DUT, in the n-side at the most irradiated point (y=4.2cm) at a bias voltage of 120V for the normal incident pions. The efficiency was defined by the existence of a hit within a window (± three 50μ-strips) around the interpolated point from the upstream and the downstream anchor hits or clusters. The cluster was defined when the hit strips were consecutive; the cluster-center was the geometrical center of the hit strips in a cluster. Only one cluster was allowed in each anchor planes. Below 1.5 fC the efficiencies were essentially 100%. Above 1.5 fC the efficiency started to decrease and reached 50% at above 3 fC: 3.1 fC (50μ pitch), 3.5 fC (over 100μ pitches). The 50% point is the median pulse height of the energy deposition (Landau distribution). The observation was consistent with that the lower tail-end was about half of the median pulse height.

The electronic noise behavior can be expressed by occupancy, i.e., the noise hit rate of a single strip. The occupancy was evaluated for the strips more than ± six 50μ-strips away from the interpolated track points, and is shown in Fig. 5(b) as a function of the threshold. There were two components in the distribution: (1) intrinsic electronic noise which was increasing exponentially below 1 fC, (2) nearly flat distribution above 1 fC at a level of $10^{-4}$. The source of this flat distribution is yet to be identified. The occupancy at one sampling before the triggered sampling showed an ideal fall-off of the intrinsic noise down to $10^{-6}$ over 1 fC. This indicated that the source of the noise was correlated with the hits and not an accidental coincidence.

A scatter plot of the efficiency vs. noise occupancy is shown in Fig. 6. The noise occupancy broke off at a level of $10^{-4}$. Since the efficiency was still high at the thresholds where the noise occupancy broke, the knee of the break-off was at 90 degrees.

The bias dependence of the efficiency is shown in Fig. 8(a). The threshold was fixed at 1 fC and the bias voltage was varied from 20 to 150V. The efficiency in the n-side was high, while that of the p-side was low. This was a clear indication that the p-n junction was in the n-side. There was little difference in the efficiency in the different pitches in the n-side; a large difference in the p-side.

This can be understood from the median pulse height distribution shown in Fig. 8(b), obtained from the 50% points of the threshold scans at the bias voltages. The n-side median pulse heights were saturating above 120V; decreasing slowly with decreasing bias voltage. The p-side median pulse heights were much smaller; decreasing from much higher bias voltages. These can be explained by granting the bulk was inverted from the n-type to the p-type. The variation of the n-side median pulse height was well expressed by the variation of the depletion depth in the bulk in the bias voltages below 120V, which was proportional to a square-root of bias voltage. The wider pitches collected more charges than the 50μ pitch: more than 10% in the n-side, much more in the p-side.

Since the lower end of the Landau distribution is half of the median, signals in all pitches were essentially all above 1 fC in the n-side, even at 40V. There was little difference in the efficiency in the 50μ, 100μ and 150μ pitches. In the p-side, the signals were small and a large difference in the pulse height made the large difference in the efficiency.

Fig. 5 (a) Efficiency and (b) occupancy as a function of threshold for the normal incident pions. The data were collected for the n-side of the irradiated LBIC-DUT at y=4.2cm and at a bias voltage of 120V. Responses of three pitches are shown: 50μ (circle), 100μ (cross), and 150μ (diamond).

Fig. 6 Efficiency vs. noise occupancy in the irradiated LBIC-DUT at y=4.2cm and at a bias voltage of 120V in the n-side: 50μ (circle), 100μ (cross), 150μ (diamond).

The data showed that a pulse height difference in the n-side in the 50μ and over 100μ pitches was more than 10%. A part of the difference can be understood with a signal simulation program[15] which has included: (1) the effect of inducing the charges in the readout strips by the movement of the electrons and holes, and (2) a ballistic deficit by a fast shaping amplifier. The program has explained the pulse height difference of about 3%. The rest could be explained by the charge spread due to a capacitive coupling between the strips (i.e., interstrip capacitance), which is not implemented in the version used here. There was a larger charge spread in the p-side in the partially depletion voltages where the undepleted region spread between the readout strips and the depleted region in the bulk. A comparison of the non-irradiated and the irradiated LBIC-DUT can be found in detail in the ref. 9.

Fig. 7 (a) Efficiency at a threshold of 1fC and (b) the median pulse height distribution as a function of bias voltage for the normal incident pions. The data was collected for the irradiated LBIC-DUT at y=4.2cm: 50μ (circle), 100μ (cross), 150μ (diamond) in the n-side; 50μ (square) and 100μ (triangle) in the p-side.

## ANGULAR DEPENDENCE

### A. *Efficiency*

When particles hit the silicon strip detector in angle (the $\phi$ incident angle perpendicular to the strips), the generated electron-holes pairs can be split into two regions sensitive to different strips. This leads to smaller collected charges and, depending on the threshold, inefficiency.

The angular dependence of the efficiency at the 1 fC threshold of the non-irradiated LBIC-DUT is shown in Fig. 8: (a) in the n-side, and (b) in the p-side at a bias voltage of 100V, which voltage was about 30V above the depletion voltage of the non-irradiated detector. The 50μ pitch was fully efficient above 20° and over 100μ pitches above 35°. The n-side was slightly inefficient in larger angles than in the p-side. The angular dependence of the irradiated DUT is shown in Fig. 9(a) and (b), at 120V, which voltage was about the depletion voltage. The same trend was observed in the n-side. In the p-side, the 50μ pitch showed a large inefficiency. The 100μ pitch was, on the contrary, fully efficient.

The behavior (of the irradiated detector) can be understood from the angular dependence of the median pulse height shown in Fig. 10. In the n-side, the median pulse height decreased as the incident angle increased. The larger pitches (100μ and 150μ) had a smaller slope than that of the 50μ pitch. The effect was basically geometrical. At 30° a tack traverses 170μm over 300μm thick silicon, i.e., a track is splitting into three 50μ-strips. The excess of the pulse height, e.g., 50% over the 1/3 of pulse height of the normal incidence in the 50μ pitch at 30°, could be attributed to: (1) 15% increase of track length, (2) contribution from the charge spread of about 15% (observed in Fig. 7(b)), and (3) partial depletion depth less than 300μm, which precise information was not available from the data. In the larger pitches, splitting of the charges into less strips gave the smaller slopes. In the p-side, the angular dependence was much smaller due to a larger charge spread than that of the n-side. In the efficiency plot, there was little loss as long as the median pulse height was above 2 fC for the efficiency at the threshold of 1 fC.

In the case of partial depletion, the signals will be lost due to less depletion depth than 300μm. The angular dependence of the efficiency can be estimated by combining the Fig. 6(b) and the Fig. 10. As described in the introduction, the particle of 1 GeV/c momentum will hit the silicon strip detectors at an incident angle of 10° + tilt angle of the detector at the radius of 60cm. For a case of the tilt angle of 7°, the 50μ pitch is fully efficient even for a slightly partially-depleted operation; the 100μ pitch is fully efficient for well partially-depleted operation.

Fig. 8 Angular dependence of the efficiency at the threshold of 1fC for the non-irradiated LBIC-DUT at a bias voltage of 100V: (a) in the n-side: 50μ (circle), 100μ (cross), 150μ (diamond) pitches; (b) in the p-side: 50μ (circle), 100μ (cross) pitches.

Fig. 9 Angular dependence of the efficiency at the threshold of 1fC for the irradiated LBIC-DUT at a bias voltage of 120V at y=4.2cm: (a) in the n-side: 50μ (circle), 100μ (cross), 150μ (diamond) pitches; (b) in the p-side: 50μ (circle), 100μ (cross) pitches.

Fig. 10 Angular dependence of the median pulse height of the irradiated LBIC-DUT at the bias voltage of 120V at y=4.2cm: (a) in the n-side: 50μ (circle), 100μ (cross), 150μ (diamond) pitches; (b) in the p-side: 50μ (circle), 100μ (cross) pitches.

### *B. Spatial resolutions*

Another fundamental output from the detector-FEE chain is the spatial resolution of the silicon strip detector. The spatial resolution was derived from the deviation of the hit or cluster in the DUT from the interpolated position from the upstream and the downstream anchors. The hit or cluster was limited within the efficiency window (± three strips) in the DUT. The sigma of the deviation was obtained in two ways: (1) in T330, the r.m.s. of the deviation was calculated successively by eliminating the points which were out of 3 sigma's until the r.m.s converged, (2) in T355 the sigma was obtained by fitting a Gaussian to the Gaussian-smeared (with a small sigma) distribution after eliminating the over 3 sigma points once. The reason to apply these methods was that the deviations were quantized because the hits were quantized in the strip pitches. A straight-forward Gaussian fitting did not work because there were zero's between the quantized points. The method (1) would give a smaller sigma while the method (2) would give a larger one. The difference would be the amount of systematic error involved in the estimation of resolutions.

Fig. 11 Spatial resolutions at the threshold of 1fC: (a) the non-irradiated LBIC-DUT at a bias voltage of 100V, 50μ (circle), 100μ (cross), 150μ (diamond) pitches in the n-side, 50μ (filled circle), 100μ (filled square) in the p-side; and (b) the irradiated LBIC-DUT at a bias voltage of 120V and at y=4.2cm, the same designations for the pitches and the marks.

The point spatial resolution was obtained from the deviation sigma as in the following. (1) For the regions where the pitches of the DUT and the anchors were same, i.e., in the 50μ and 100μ pitches, the point spatial resolution was calculated by multiplying the factor $\sqrt{9/14}$ out of the triplet of 1:2 distance. The difference of non-irradiated and irradiated detectors was ignored. (2) For the DUT pitches other than the 50μ and the 100μ, the spatial resolution was obtained by subtracting the anchor resolutions obtained in (1) from the deviation sigma. The angular dependence of resulting spatial resolutions of the non-irradiated LBIC-DUT is shown in Fig. 11(a) and those of the irradiated in Fig. 11(b).

The resolutions at the normal incidence were basically consistent with the expected $pitch/\sqrt{12}$ in the non-irradiated and the irradiated cases. In the angular dependence, the minima of the resolutions were observed at the angles of $\tan^{-1}(pitch/thickness)$ where the maximum charge splitting into the adjacent two strips were expected. There were slight degradation of resolutions in the irradiated data over the non-irradiated one, which source would be the systematic error in the estimation described in the above and/or a real degradation by the radiation damage. The resolutions in the p-side were slightly better than those of the n-side in the non-irradiated while those of the n-side were better than those of the p-side in the irradiated detector, which was consistent with that the side of the p-n junction was better. The 50μ pitch lost resolutions above 20° coinciding with the loss of the efficiency above the angle.

In the ATLAS silicon strip detector, the maximum incident angle is less than 20° and, thus, a detector with any pitches is expected to work. If 90° strips were to be used, e.g., in a vertex layer where a particle will hit at a maximum angle of 50°, a pitch of more than 100μ is required above the angle of 25°.

### *C. Effective spatial resolution*

As seen in Fig. 11, the spatial resolution was improved over the $pitch/\sqrt{12}$ for the tracks at the angle of $\tan^{-1}(pitch/thickness)$. This can be explained by the sharing of charges into two adjacent strips, thus splitting of a pitch into a single hit and a double hit regions. If the strip pitch (width=$P$) is split into a single hit region 1(width=$H$) and a double hit region 2(width=$W$), as shown in Fig. 12, the effective resolution will be

$$\sigma^2 = \frac{1}{N}\sum\left(x-\bar{x}\right)^2 \qquad (1)$$

$$= \frac{n}{N}\left[\frac{1}{n}\sum\left(x-\overline{x_1}\right)^2\right] + \frac{m}{N}\left[\frac{1}{m}\sum\left(x-\overline{x_2}\right)^2\right]$$

$$= \frac{n}{N}\sigma_1^2 + \frac{m}{N}\sigma_2^2$$

$$= \left(\frac{P}{\sqrt{12}}\right)^2\left[\left(1-\frac{W}{P}\right)^3 + \left(\frac{W}{P}\right)^3\right] \qquad (2)$$

where $x$ symbolizes the track position, $\bar{x}$ the center of the hits, $n$ the number of tracks in the region 1, $m$ the number of tracks in the region 2, and $N$ the number of total tracks in the pitch $P$. The improvement factor is the function of the width $W$; the resolution is halved when $W = H = P/2$. The improvement from 14μm to 12μm in the 50μ pitch in Fig. 11 indicated the double-hit width was about W/P=10% at the threshold of 1 fC. Although the charges were maximally shared in two strips in the $\tan^{-1}(pitch/thickness)$ angle, the threshold of 1 fC was too high to pick the smaller signals, thus leaving the narrow region where the charges were split nearly equally.

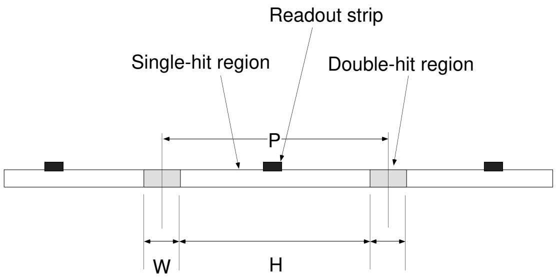


Fig. 12 A schematic drawing of the splitting of a pitch into a single-hit and a double-hit regions.

## INTERMEDIATE-FLOATING-STRIP READOUT

### A. *Efficiency and occupancy*

One way to create the double-hit region intentionally is to put an extra strip in the middle of the readout strips. This was done in the case of one intermediate floating strips, 100*μ. The intermediate strip had the bias voltage on the implant, thus collecting charges to the strips. Since no amplifier was connected to the readout electrode, the collected charge had to be divided into the neighboring strips, which were grounded or connected to the amplifier (i.e., virtually grounded), according to the inter-capacitance. In the DUT geometry, where the strips were narrow to reduce the interstrip capacitance, there were nearly equal coupling capacitances to each of the adjacent neighbors and to the backplane. One neighbor would see about 1/3 of the charges collected in the floating intermediate strips. A real design can be optimized by balancing the maximum coupling to the neighbors and the minimum noise increase by the capacitance. An extreme design of this sort is the charge division readout by inserting more intermediate strips and reading out the amount of charges by an analog readout electronics.

The efficiency of the 100*μ case is shown in Fig. 13 as a function of the threshold for the irradiated detector, at y=4.2cm at a bias voltage of 120V for the normal incident pions. The shape of the distribution was quite different from that of no-intermediate case shown in Fig. 5(a): there was a kink at a threshold of 1.5 fC. The distribution above 1.5 fC can be understood to come from the single-hit region around the readout strip while below 1.5 fC from the double-hit region. The efficiency reached 100% at a threshold of 0.7fC which was a half of the no-intermediate case.

The noise occupancy is also shown in the Fig. 13. The occupancy was about equal to that of the 50μ case. This was more than the expected noise for the 100*μ case where the interstrip capacitance would be halved due to the series connection of the basic 50μ-pitch interstrip capacitances.

Fig. 13 Efficiency(circle) and noise occupancy(cross) distributions of the 100*μ case in the n-side of the irradiated detector as a function of the threshold at y=4.2cm and at a bias voltage of 120V for the normal incident pions.

### B. *Local Median Pulse Height distribution*

Since the total efficiency was the sum of the single-hit and the double-hit, the region of one pitch of the 100*μ case was required to be mapped out. The DUT could be measured at a quantization step of 8.3μm. This was because: the pitch of the anchor of the 100*μ case was 50μ and the quantization in one anchor plane was 25μm, combination of two anchors in the 1:2 separation to the DUT made the interpolated positions in a step of 8.3μm. By binning the efficiency distributions as a function of threshold in the 8.3μ steps, a local median pulse height distribution was derived as shown in Fig. 14. The unit of the horizontal axis was the 50μ-pitch strips: the positions 0 and 2 were where the intermediate strips were and the position 1 the readout strips. There was a offset in the distribution due to an alignment of the anchors and DUT.

Fig. 14 Local median pulse height distribution in one pitch of the 100*μ case in the n-side of the irradiated detector at y=4.2cm at a bias voltage of 120V for the normal incident pions.

Two regions were clearly observed: an area of a full charge collection of 3.4 fC at the readout strips and an area of less charge collection, about 1/3 of the full charge, in the intermediate strip regions. The boundary of the regions was smeared out, attributed to a charge spreading. The threshold dependence of the efficiency in Fig. 13 can be understood from the local median pulse height distribution.

## *C. Spatial resolution*

The spatial resolution of the 100*μ case(circle) is plotted in Fig. 15 as a function of the threshold together with those of the no-intermediate strips: the 50μ(cross) and the 100μ(diamond). Both the 50μ and the 100μ showed a small improvement in the resolution as the threshold was lowered below 1 fC. This was the effect of picking up a wider double-hit region in the middle of the readout strips. Below a very low threshold the resolutions were quickly getting worse due to the contribution of the intrinsic electronic noise.

The 100*μ case showed a large improvement in the spatial resolution: nearly from the resolution of the 100μ at the threshold of 1 fC down to close to that of the 50μ at 0.5 fC, much larger improvement than those seen in the no-intermediate 50μ or 100μ cases. No further improvement was observed below 0.5 fC because of the noise contribution. Over 1 fC in the 100*μ case, the resolution started to be improved again. This was an superficial effect due to the loss of efficiency.

The whole behavior can be understood as in the following. When the threshold was very low, the whole pitch, i.e., 100μ, was sensitive and the spatial resolution would be ideally halved due to the splitting of the single-hit and the double-hit regions. As the threshold was getting higher, one of the double-hits was lost and the whole pitch became a single-hit region, thus the spatial resolution would reach that of the readout pitch. In the threshold further higher, both signals in the double-hit region were lost and only the region around the readout strips was sensitive, thus resulting the spatial resolution being that of 50μ.

Fig. 15 Spatial resolutions as a function of threshold of the floating-intermediate-readout 100*μ case(circle), the no-intermediate 50μ(cross), and the 100μ (diamond) in the n-side of the irradiated detector at y=4.2cm and at 120V for the normal incident pions.

## *D. Angular dependence of efficiency and resolution*

The incident angle dependence of the efficiency, etc. could be interesting because a segment of a track, which was in the double-hit region for the normal incidence, would get into the single-hit region because of the inclination and the efficiency would be increased. The efficiency distributions as a function of the incident angle ($\phi$ angle) are shown in Fib. 16(a) for two thresholds: at 0.6 fC(circle) and at 1.0 fC(cross). The improvement of the efficiency was observed in the 1fC case: 88% at 0° to >99% around 20°. The corresponding spatial resolutions are shown in Fig. 16(b). The spatial resolution got better where the efficiencies were higher in the angles over 20°. In the 0.6fC threshold, the efficiencies were essentially 100%; losing a bit around 20° where the resolutions were slightly worse than those at the higher efficiencies.

Fig. 16 (a) Efficiencies and (b) spatial resolutions as a function of incident angles for two thresholds: 0.6 fC(circle) and 1.0 fC(cross), in the 100*μ configuration.

## *E. Enhancement to a binary electronics*

In the floating-intermediate-strip readout, the improvement of the spatial resolution was limited by the intrinsic noise of the front-end amplifier . There are two ways to improve the situation: (1) to use a amplifier with lower noise, (2) to add a circuitry to suppress the noise. The former is already difficult: the present electronics was barely fulfilling the requirement to be efficient and low occupancy for the no-intermediate readout.

One idea for (2) is to add two thresholds, high and low, and a neighbor logic of AND and OR as shown in Fig. 17[16]. When the signals are high, i.e., the signals are in a single-hit region, the signals pass through the high threshold, much like the no-intermediate readout and a threshold. When the signals are in the double-hit region, the signals are picked up by the low threshold in the neighboring channels. Without further circuitry, the low threshold can not be lowered because of the intrinsic noise. With the two-fold coincidence (AND circuitry) of the output of the low thresholds, the intrinsic noise can be suppressed to a squared level because it is random. The output of AND is fed back into neighboring channels through the three-fold OR logic to keep the information and to keep the number of output channels constant. This circuitry can also enhance efficiency and resolution in the double-hit region in the no-intermediate readout scheme.

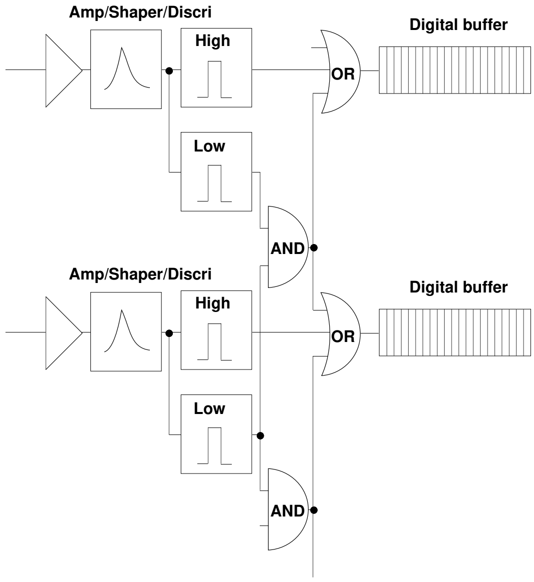


Fig. 17 An idea to enhance a binary readout electronics utilizing two thresholds (high and low) and a neighbor logic (AND and OR circuitry).

## MEASUREMENT OF HALL MOBILITY

The swath of electron and hole pairs along a passage of charged particles in 300μm thick silicon splits into more than single strips by incident angles ($\phi$-angle) or by the deflection of carriers in a magnetic field (Hall effect). The effect can be observed as a change in the fraction of multiple-strip hits. The distributions of the multi-hit fraction were measured in the beam test T280 for a non-irradiated detector with and without a magnetic field[17]. A clear dependence on the incident angle and on the magnetic field were observed as shown in Fig. 17: (a) in the null ($B$=0T) and (b) in the 1.0 Tesla field ($B$=1T). The n-side fraction was higher than that of the p-side, possibly for the charges being spread over strips due to a larger interstrip capacitance.

The minimum in the $\phi$-angles corresponds to the Hall angle of a carrier where the Hall effect is canceled out by the incident angle. A hyperbolic function, $y = c\sqrt{1+(x-a)^2/b}$ was fitted to the data to extract the minimum. The offset in the $\phi$-angle were calibrated using the $B$=0T data. From the $B$=1T data, the Hall angles ($\theta_H$) for the electrons and the holes were obtained to be +7.87±0.24° (electrons: n-side) and -1.85±0.17° (holes: p-side). The corresponding Hall mobilities were $\mu_H^e$=1391±43 cm/s/(V/cm) (electrons) and $\mu_H^h$= 325±30 (holes) using the relation $\tan\theta_H=10^{-8}\mu_H B$. The dopant concentration of the silicon was estimated to be $(1.02\pm0.15)\times10^{12}$ cm$^{-3}$ from a measurement of the depletion voltage of the non-irradiated detector.

Fig. 18 Multi-strip hit fraction as a function of the $\phi$-angles: (a) $B$=0T, (b) $B$=1T; n-side (circle/solid line), p-side (cross/dashed line). The minimum was obtained by fitting a hyperbolic function to the data (overlaid curves).

## SUMMARY

A double-sided silicon strip detector with a radiation-tolerant design, and an improved version, were fabricated and characterized in a sequence of at KEK using 4 GeV/c pions. The detectors were combined with newly designed fast, lower power, bipolar amplifier-shaper-discriminator chips and CMOS digital pipeline chips to record hit-no hit signals in the strips (binary readout scheme). The analog signal processing and the digital buffering proceeded simultaneously at a clock of 40 MHz. Three were successfully carried out: T280 for proof of principle of the detector and the front-end electronics and a data taking with and without a magnetic field, T330 for the improved double-sided detector and a faster electronics before irradiation, and T355 for the same detector in the T330 after irradiation to the protons to an equivalent fluence of $1\times10^{14}$ p/cm$^2$.

Efficiencies, noise occupancies, spatial resolutions were measured by varying the bias voltage to the detector and varying the threshold of the binary electronics. The observables were measured in the n-side and the p-side simultaneously in the double-sided detector. Comparison of the non-irradiated and the irradiated detector showed clear consequence of the bulk type-inversion from the initial n-type to the p-type after irradiation. The high-efficiency side moved from the p-side to the n-side. The median pulse height of the charge deposition (Landau fluctuation) were extracted from the threshold scan of the efficiencies. The charge collection in the n-side of the irradiated detector decreased as a function of bias voltage as expected for the partial depletion of the bulk. The variation of the pulse height was consistent of the variation of the depletion depth developed from the n-side. The proton irradiation was non-uniform in the detector. There were regions where type was well-inverted, intrinsic, and non-inverted in the detector. Despite the non-uniformity, the detector worked without any failure.

Incident angle dependence were extracted for the efficiencies and the resolutions in several pitch configurations: 50μ (basic pitch), 100μ (two-gang), and 150μ (three-gang). The detector strips were connected to the readout electronics by ganging the strips into a readout channel with wire-bonding. The angular dependence was consistent basically with geometrical effect, in addition to a plausible charge spreading. The spatial resolutions were consistent with $pitch/\sqrt{12}$ as long as the efficiencies were high at the threshold. There was a small improvement where the charge sharing was maximum in the angles defined by the pitches and the silicon thickness.

The effect of charge division was evaluated in a one intermediate-floating -strip readout of 100*μ pitch. The configuration showed an improvement in the spatial resolution being understood as making a separation of a single-hit and a double-hit regions. Although an improvement was observed, the noise level of the amplifier was prohibitive to use the scheme.

Angular dependence of the multi-hit fractions in a 1 Tesla magnetic field enabled to extract the Hall mobility of the electrons and the holes in the high resistivity silicon: $\mu_H^e$=1391±43 cm/s/(V/cm) (electrons) and $\mu_H^h$= 325±30 cm/s/(Vcm) (holes) for a dopant concentration of $(1.02\pm0.15)\times10^{12}$ $cm^{-3}$.

## REFERENCES


[1] Presentations in these proceedings: M. Tyndel, ATLAS; J. Spalding, CDF; R. Wheadon, CMS; P. Gutierrez, D0; P. Collins, DELPHI; T. Matsuda, KEK-B; R. Johnson, SLAC-B; A review for LEP detectors: A. Schwarz, Nucl. Instr. Meth. A342(1994)218

[2] ATLAS Silicon strip detectors, cf. ATLAS Technical Proposal, CERN/LHCC/94-43, Dec. 1994

[3] L.R. Evans, "The Large Hadron Collider", submitted to the 1995 Particle Accelerator Conference, Dallas, 1-5 May, 1995

[4] T. Ohsugi et al., Nucl. Instr. Meth. A342(1994)22; T. Ohsugi et al., in these proceedings.

[5] T. Ohsugi et al., Nucl. Instr. Meth. A342(1994) 16, and an improvement afterward.

[6] E. Spencer et al., IEEE Trans. Nucl. Sci. 42(1995)796

[7] Y. Unno et al., KEK PS experiment proposals (test beam): T280: March 4 - March 9, 1993; T330: June 2 - June 9, 1994; T355: Feb. 23 - March 2, 1995

[8] J. DeWitt et al., IEEE Trans. Nucl. Sci., 42(1995)445

[9] Y. Unno et al., "Characterization of an irradiated double-sided silicon strip detector with fast binary readout electronics in a pion beam, to be published in IEEE Trans. Nucl. Sci., 43(1996)

[10] J. DeWitt, "A Pipeline & Bus Interface Chip for Silicon Strip Detector Read-Out", 1993 IEEE Conference record, vol.2, p749

[11] D. Dorfan, Nucl. Instr. Meth. A342(1994)143

[12] H. Spieler, Nucl. Instr. Meth. A342(1994)205

[13] A. Fry and M. Nomachi, "UNIDAQ: a portable data-acquisition system for SSC detector R&D", 8th Real-time Computer Applications in Nuclear, Particle, and Plasma Physics (RT93), June 8-11, 1993, Vancouver, Canada

[14] B. Hubbard et al., "A Digital Readout Sequencer (DRS)", SCIPP 93/43, Univ. of California, Santa Cruz

[15] J. Leslie, A. Seiden, Y. Unno, IEEE Trans. Nucl. Sci., 40(1993)557

[16] An idea generated through a discussion between Y. Unno and W. Dabrowski, FPNT, Cracow, Poland. A circuit simulation and implementation are being carried out by W. Dabrowski.

[17] Y. Unno et al., "Beam Test of the SDC Double-sided Silicon Strip Detector", 1993 IEEE Conference Record, vol.1, p38